JOURNAL OF GUIDANCE, CONTROL, AND DYNAMICS
Vol. 29, No. 1, January–February 2006

Control and Maneuverability of a Square Cross-Section Missile

John R. Cleminson*
QinetiQ, Ltd., Farnborough, England GU14 0LX, United Kingdom
and
Rick A. Hyde†
University of Bristol, Bristol, England BS8 1TR, United Kingdom

A study has been conducted into the aerodynamics, control, and performance of a square cross-section supersonic missile. Comparisons have been made with an equivalent circular cross-section baseline. This paper summarizes the control and maneuverability findings and explores the relationship between airframe asymmetry and autopilot architecture. Missile autopilot designs based on classical, H_∞, and nonlinear dynamic inversion methodologies are compared in terms of a robust stability requirement defined by Nichols exclusion regions, applied in a multiloop sense. Valuable insights into the required autopilot architecture are gained through this. Various other performance metrics are also proposed and used to explore the relative merits of the square cross-section body shape.

Nomenclature

a_y, a_z	=	achieved accelerations, to starboard and down, in the control frame
a_{yc}, a_{zc}	=	acceleration commands into the steering function, in the control frame
a_{yd}, a_{zd}	=	acceleration commands into the autopilot, in the control frame
C_{L0}, C_{M0}, C_{N0}	=	nondimensional moment coefficients for the body with undeflected fins
C_{X0}, C_{Y0}, C_{Z0}	=	nondimensional force coefficients for the body with undeflected fins
D	=	reference length for both airframes
$I_{xx}, I_{yy}, I_{zz}, I_{xy}, I_{xz}, I_{yz}$	=	standard inertia matrix terms
J	=	inertia matrix
K_∞	=	H_∞ loop-shaping compensator
k_{ay}, k_{az}	=	autopilot acceleration error gains
k_p, k_q, k_r	=	autopilot angular rate feedback gains
$k_{\text{synp}}, k_{\text{synq}}, k_{\text{synr}}$	=	autopilot synthetic gains
p	=	roll rate, in the control frame
p_d	=	roll-rate demand, in the control frame
Q	=	dynamic pressure
q	=	pitch rate, in the control frame
r	=	yaw rate, in the control frame
S_{ref}	=	reference area, $= \pi D^2/4$ for both airframes
v	=	lateral velocity, in the control frame (positive starboard)
w	=	vertical velocity, in the control frame (positive down)
x_{aero}	=	position of aerodynamic reference behind the nose (negative)
x_{cg}	=	position of the centre of gravity behind the nose (negative)
$\Delta C_\xi, \Delta C_\eta, \Delta C_\varsigma$	=	nondimensional moment increments caused by fin deflections
δ	=	complex number used to denote uncertainty
ε_{ncf}	=	normalized coprime factor robustness
ε_μ	=	robustness measured
ζ	=	rudder collective fin deflection
η	=	elevator collective fin deflection
λ	=	aerodynamic roll angle
μ	=	structured singular value
ξ	=	aileron collective fin deflection
σ	=	total incidence
Ω	=	angular velocity vector $[p \;\; q \;\; r]^T$
ω	=	frequency, radians/s

Introduction

FUTURE missiles might have noncircular cross sections to obtain better aerodynamic performance and/or greater volumetric efficiency or for the sake of airbreathing propulsion, special sensors, or stealth.

Much of the previous research work that is reported in the literature on missiles with noncircular cross sections has focused on body alone.[1] Nevertheless, there are exceptions in which realistic configurations, that is, those with lifting and control surfaces, have been considered. For example, work has been done in the United States on lifting-body airframes with highly elliptical cross section[2] and on the triangular-like Have Dash II.[3] Work has also been conducted in Sweden on airframes with triangular cross section.[4] Because of their shapes, such airframes are difficult to evaluate rigorously against traditional four-fin circular cross-section configurations. Moreover, the control solutions for them have tended to presume bank-to-turn (BTT) steering,[5–7] whereas this might not always be the best policy for achieving high maneuverability.[8–10]

Some missiles with noncircular cross sections are already in service. Again, these tend predominantly to use BTT steering and have fairly low maneuverability, for example, the typical subsonic bus vehicle or cruise missile. When high maneuverability is required, it is important to consider steering laws that include at least an element of skid to turn (STT). Hence, for circular and noncircular airframes alike, it is important to consider autopilot design, stability, and performance in an all-round-the-body sense.

This paper summarizes the control and maneuverability findings of a study that investigated a supersonic rocket-propelled missile with a square cross section. To make sense of the findings, comparisons were made at every stage with an equivalent circular cross-section baseline. The configurations are illustrated in Fig. 1. Computational fluid dynamics (CFD) was used to generate

Received 12 August 2004; presented as Paper 2004-5329 at the AIAA Guidance Navigation and Control Conference, RI, 16–19 August 2004; revision received 4 May 2005; accepted for publication 13 May 2005.

*Senior Research Scientist, Cody Technology Park, Hants; jrcleminson@qinetiq.com.

†Lecturer, Department of Mechanical Engineering; rick.hyde@bristol.ac.uk.

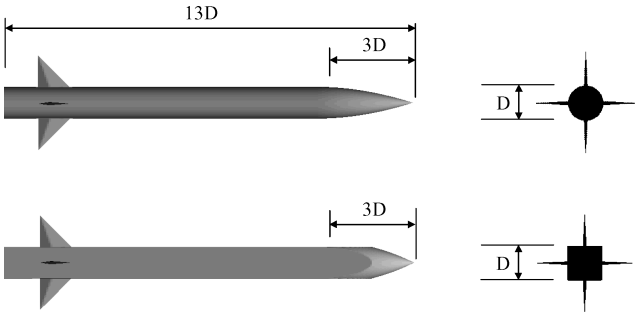

Fig. 1 Configurations of the circular and square airframes.

aerodynamic data. The fact that sufficient data were generated for detailed control and performance analyses is thought to be unprecedented. Details of aerodynamics aspects are reported elsewhere.[11,12]

Several autopilot methodologies and steering laws were considered. This was done to help understand how autopilot architecture should depend on the aerodynamics and to exploit fully the potential of the airframes for maneuverability. Again, comparisons were made against baselines: the baseline autopilot design was selected as the standard classical three-loop autopilot,[13] and the baseline steering law was that of traditional STT.

At the outset it was reasoned that a square cross-section airframe is likely to introduce additional cross couplings that require mirroring in the autopilot architecture. With its decoupled architecture, the standard classical three-loop autopilot does not readily permit this (in a general sense, although practical versions often do have cross-channel paths inserted to compensate for specific aerodynamic terms and coupling caused by roll rate). For cross-coupled systems, the control community has developed a number of solutions for design and analysis. Two such methods were considered here, namely, H_∞ and nonlinear dynamic inversion (NDI). The H_∞ paradigm is supported by a number of design methods, one of the most successful being the loop-shaping approach based on normalized coprime factors.[14] This has been applied in a number of applications and was first flight tested in full gain-scheduled form on a Harrier jump-jet[15,16] and also on rotorcraft.[17,18] More recently, there has been increased interest in the NDI approach,[19] as it provides a more intuitive and simple architecture to implement.[20,21]

In addition to the baseline STT steering law, the study considered STT-45BTT and 180BTT schemes, among others. This paper defines these three laws. The autopilot designs were not influenced by the choice of steering, that is, there were no presumptions of restricted incidence on account of the steering.

Several metrics are proposed and have been used to assess the stability and performance of the airframes. One of these represents a multivariable stability measure and is based on an extension of single-loop Nichols exclusion regions, as typically used for military aircraft.[22] Using the method of structured singular value,[23] multiloop Nichols-based uncertainty can be applied.[24] Another metric is the maximum trim capability as a function of incidence orientation around the body. This provides an indication of the steady-state acceleration that can be achieved with an airframe, before the consideration of a steering law. A third metric is the effective time constant, which provides a measure of responsiveness, that is, of how quickly a demand in a particular direction is achieved. A fourth metric is what is referred to here as the maneuver reach capability, which provides information about the points in space that are reachable from a given starting point.

This paper makes two main contributions. The first is the comparison of the effects of airframe shape, autopilot methodology, and steering law on stability and maneuverability, as indicated by the proposed metrics. The second is the additional insight that is provided into the autopilot methodologies, in terms of constraints imposed by the respective architectures and some practical issues of implementation.

The paper is organized as follows. First, the airframe configurations are introduced, and the various assumptions about mass properties, subsystem dynamics, etc. are discussed. Next, the maximum trim capabilities are compared, and the uncontrolled-airframe stability characteristics are explored. Then, the robustness requirements are defined, and the stability metric is introduced. The autopilot designs are developed for each airframe, and relative merits in terms of simplicity of implementation are discussed. Each autopilot design on each airframe is then evaluated in terms of the stability metric. Steering laws and the effective time-constant metric are then defined, and results are presented for these. Finally, the maneuver reach capabilities of the airframes are examined for one autopilot design and selected steering laws.

Airframe Configurations and Operating Conditions

Airframe Configurations

At an early stage it was decided that the configurations selected for study should be supersonic and rocket propelled (not necessarily generating thrust) and have rear control fins. Compared with subsonic, airbreathing, and/or canard-controlled missiles, such configurations are more feasible from the point of view of generating large aerodynamic data sets using CFD. Airbreathing missiles also present additional constraints on incidence, etc., which we did not wish to consider during this research.

A traditional four-fin circular cross-section airframe with the preceding desired characteristics was obtained from Royal Aircraft Establishment archives to represent the baseline. Additionally, this configuration came with a fairly comprehensive—though not a complete—set of experimental aerodynamic data with which to help validate and give confidence in the CFD predictions.

The square cross-section configuration was made highly comparable with the circular baseline, as though it had evolved from it. In particular the overall lengths were made the same, the width of the side of the square was made equal to the circular diameter D, and the fin arrangements were made identical. To have the same tip-to-tip span, the fins of the square configuration were side mounted rather than corner mounted. This also avoided issues about the potential loss of control effectiveness caused by the root gap that could occur with deflected corner-mounted fins. The resulting configurations are shown side by side in Fig. 1.

Both airframes have circular cross-section noses of essentially tangent-ogive profile[11] and length $13 \times D$. In the square case, the nose is tangential with the body only at the corner points, and thus the apex angle is greater by a factor of $\sim\sqrt{2}$. The circular cross-section nose was considered better than square from a seeker perspective, and it served to simplify wind-tunnel model manufacture. Nevertheless, this nose in conjunction with the square body was not expected to be aerodynamically optimal.

A wind-tunnel model of the square cross-section airframe was manufactured under the study and tested by NASA Langley Research Center under the auspices of The Technical Cooperation Programme. Again, this provided an excellent source of validation for the CFD predictions.

In this study the approach taken was to make the square configuration geometrically comparable with a circular baseline. The relative performance attributes of the former are influenced by its having a larger cross-sectional area and nose of lower fineness ratio. The results presented in the sequel should be viewed with this in mind.

Operating Conditions

All-round-the-body control and performance analyses require fairly comprehensive aerodynamic data sets. The generation of such sets by CFD prediction imposes a significant computational burden. Accordingly, it was necessary to restrict consideration of airframe definition and autopilot design to one Mach number. Mach 2.5 was selected, partly because measured data already existed at this condition for the circular configuration and partly because this is in the middle of the operating envelope of many supersonic missiles. Further, for the results in this paper gravity was set to zero, and

an altitude of 10 km was assumed for calculation of dynamic pressure, even in situations where the true altitude diverged from this. In this way, dependencies on missile attitude and maneuver direction relative to the Earth are avoided.

Working Assumptions and Modeling

Mass Properties

The greater volume of the square cross-section missile leads to a range of possibilities for its mass. For example, if mass were assumed to be proportional to volume, then the square cross-section missile would be a factor of approximately $4/\pi$ heavier than that of the circular cross section. This can be viewed as an approximate upper bound. An alternative assumption, which in some respects might be more realistic, would be that both missiles have the same internal configuration, that is, that of the circular, the square cross-section missile having unused space at the corners. Then, if mass differences caused by the external shapes were small, the masses and inertias would be approximately equal. In this way, the mass of the circular cross-section missile provides an approximate lower bound for that of the square configuration, albeit a bound that might not be achievable when structural and other design practicalities are taken into account. The results presented in this paper correspond to the situation where the missiles have equal mass and inertias, as comparisons are then more easily made.

The center of gravity was assumed fixed and placed in the same location for both missiles, at 47% of length behind the apex of the nose. The location was selected so that the maximum trim incidence for the square missile coincided with the maximum incidence point of the aerodynamic data. Though probably nearing the forward extreme for center of gravity, this location is regarded as not unreasonable for rockets at or near the all-burned state, such as can occur in the demanding final stages of a homing engagement. Table 1 provides a list of the mass properties that were assumed.

Subsystem Dynamics and Assumptions

The fin actuators and inertial instruments, comprising a full complement of gyros and accelerometers, were represented in both missiles, in identical fashion, as second-order lags. Fin deflection command limits were set in accordance with the maximum deflection points of the aerodynamic data, and a small amount of exceedance was permitted for transients. No rate limiting, whether on acceleration commands or within the autopilot or actuators, was considered for any of the presented results. This makes it easier to compare the effects of the differences in the airframe cross sections. The instruments were assumed stationed at the center of gravity. Table 2 specifies the relevant parameter values that were assumed.

Modeling

Designs and analyses were conducted mainly with full-force six-degrees-of-freedom models, constructed in MATLAB®/Simulink®. Because the aim at this stage was to compare the effects of basic aerodynamic differences between the circular and square airframes, rather than to consider structural and implementation issues, these were rigid-body studies in which the algorithms were represented in the continuous-time domain, ignoring any digital implementation effects. Nevertheless, as described later, constraints were placed on the autopilot designs with the need for structural attenuation in mind.

Table 1 Mass properties

Parameter	Value
D	0.2 m
Mass	125 kg
I_{xx}	0.75 kg m^2
I_{yy}	50 kg m^2
I_{zz}	50 kg m^2
I_{xy}	0 kg m^2
I_{xz}	0 kg m^2
I_{yz}	0 kg m^2
x_{cg} (relative to nose apex)	47% of $-13 \times D$ m
y_{cg}	0 m
z_{cg}	0 m

Table 2 Actuator and instrument parameters

Parameter	Value
Bandwidths of fin actuators	30 Hz
Actuation bandwidths of collectives (for design)	30 Hz
Damping ratios of fin actuators	0.7
Damping ratios of collectives (for design)	0.7
Command deflection limits	±20, deg
Gyro bandwidths	100 Hz
Gyro damping ratios	0.7
Accelerometer bandwidths	100 Hz
Accelerometer damping ratios	0.7

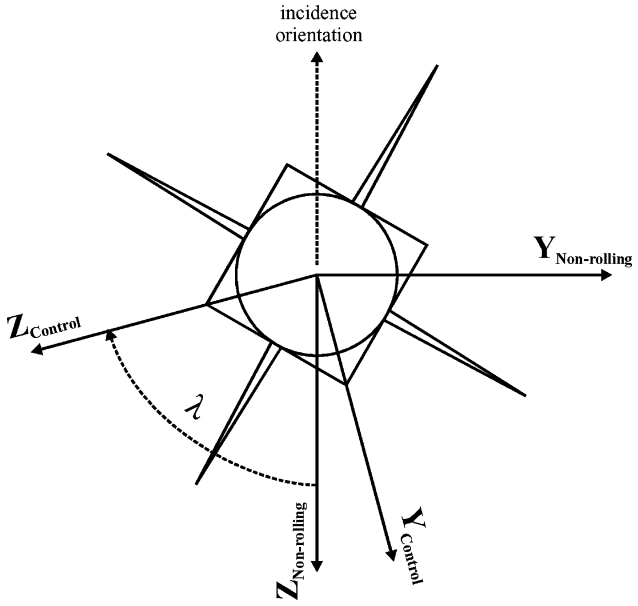

Fig. 2 Missile frames of reference.

Frames of Reference

Figure 2 defines the two frames of reference that are used in this paper and shows how they are related by the aerodynamic roll angle λ. The aerodynamic coefficients were provided with respect to the nonrolling frame, but the autopilot designs and steering laws were based on the control frame (sometimes called the rolling frame), which is body fixed. Pitch-up in the control frame occurs when $\lambda = 0$ deg and the fins are in a cross orientation (implying that the square body is orientated in a diamond).

Aerodynamic Characteristics

The aerodynamic data structure was identical for both airframes. Data sets were made available for total incidences between 0 and 24 deg, at intervals of 4 deg, aerodynamic roll angles between ±180 deg, at intervals of 7.5 deg, and collective control deflections, that is, aileron, elevator and rudder, taken to be independent of one another, in steps of 5 deg between ±20 deg. In the case of the square cross-section configuration, the data set was generated entirely by means of CFD, except for axial-force adjustments. Apart from axial force, which was biased by a constant offset, the predictions were generally in very good agreement with the experimental data gathered from the NASA tunnel test.[11,12] Nonetheless, in the worst case, at maximum incidence and 22.5 deg of aerodynamic roll angle, the nonrolling yawing moment and side-force coefficients were found to be underpredicted by ∼15 and ∼25%, respectively; likewise, the worst-case rolling moment was found to be underpredicted by ∼10%. In the circular cross-section case, CFD prediction was used to populate the aileron deflection points; the remainder of the data set being composed of the preexisting measured data. Although it was not feasible within the constraints of the study to generate a

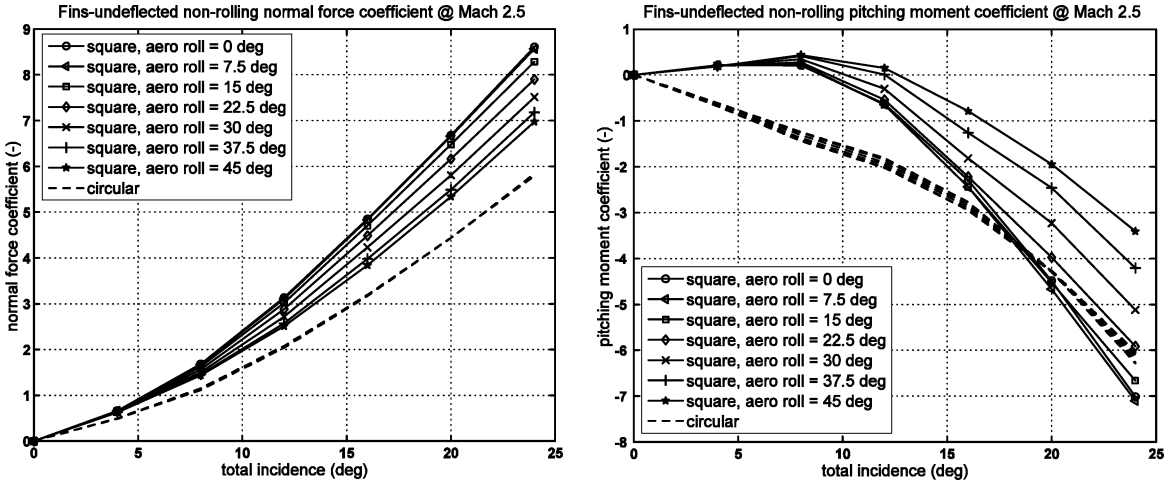

Fig. 3 Fins-undeflected normal-force and pitching-moment coefficients.

complete CFD-based data set for the circular configuration, a validation exercise was conducted, and very good agreement, with the exception of an axial force offset, was obtained between the experimental and predicted data. The preceding remarks should be borne in mind in the sequel, when relative performances are compared.

The nonrolling nondimensional force and moment coefficients, with the slight exception of the axial force, were represented as follows:

$$C_0(\sigma, \lambda) + \Delta C_\xi(\sigma, \lambda, \xi) + \Delta C_\eta(\sigma, \lambda, \eta) + \Delta C_\varsigma(\sigma, \lambda, \varsigma) \quad (1)$$

Here, λ is the aerodynamic roll angle, defined as shown in Fig. 2, and ξ, η, and ζ are the aileron, elevator and rudder collective deflections, taken about the axes of the control frame. In the case of axial force, there was an additional term for skin-friction variations with altitude. Note also that the motor was assumed to be off, so that there were no plume effects.

In spite of the different cross sections, the nondimensionalizing factors for both the square and circular cross-section data are based on the same reference area $\pi D^2/4$, and the same reference length D, where D is as defined in Fig. 1. This allows direct comparisons of the aerodynamic coefficients.

Figure 3 illustrates the fins-undeflected normal-force and pitching-moment coefficients. These are nonrolling coefficients, and the moments are taken about the center of gravity. It is seen that the fins-undeflected normal force is substantially greater in the square cross-section case: ~50% more where the planform area is a maximum with respect to the incidence orientation; where the planform area is a minimum, that is, the same area as that of the circular cross section, there is still an increase of ~20%. Additionally, the fins-undeflected pitching moment of the square cross-section airframe is generally substantially lower than that of the circular cross section, except for higher incidences around the control-frame pitch and yaw planes, where the planform area of body and fins is greatest. The square cross-section airframe is clearly statically unstable in the incidence plane at lower incidences, even with the center of gravity positioned in the moderately forward location.

Although outside the scope of this paper, it is appropriate to remark that the axial force of the square cross-section configuration is significantly greater than that of the circular.[11] This is because of the greater cross-sectional and surface areas, the greater nose apex angle, and the fact that the nose is tangential with the body only at the corners. Had the approach instead been to make equal the cross-sectional areas, it is anticipated that the axial forces would have been more similar and the normal force advantages of the square configuration would have been somewhat lower.[1]

Figure 4 shows the fins-undeflected rolling-moment coefficients, which show that the peak magnitudes are significantly greater in the square cross-section case. It is notable that in the square case, in contrast to that of the circular baseline, the sense of the roll stability changes with incidence. The natural instability of the circular cross-section airframe tends to be fastest at the higher incidences around the aerodynamic roll angles of ±45 and ±135 deg. These occur where the slopes of the fins-undeflected rolling moments are at their most adverse. A similar relationship holds for the square cross-section airframe, this time with natural instability being fastest at the higher incidences around 0, ±90, and ±180 deg. These fins-undeflected roll characteristics have a large bearing on the small-perturbation stability of the uncontrolled airframe.

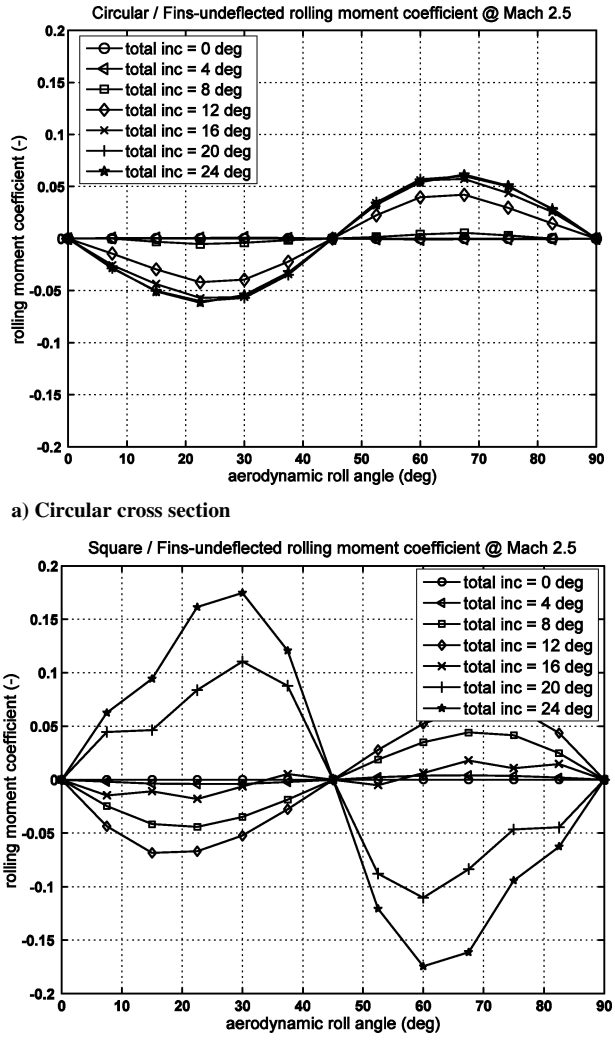

a) Circular cross section

b) Square cross section

Fig. 4 Fins-undeflected rolling-moment coefficients.

Maximum Trim Characteristics

Maximum trim capability was evaluated on the basis of maximum fin deflection. The maximum trim conditions at a given aerodynamic roll angle λ were taken as those prevailing at the first occurrence of command limiting of any of the fins. The command limits for the fins were set at the extreme deflection values of the aerodynamic data, that is, ± 20 deg. Figure 5 shows the maximum trim capability for the two airframes as a function of λ.

As expected, local peaks are evident at $\lambda = 0, 45, 90$ deg, etc., these being orientations where there is no cross coupling to counter. The greatest maximum trim capability occurs at $\lambda = 0, 90$ deg, etc., where the fins are orientated in a cross, and the square body in a diamond, relative to the incidence plane. By design, through placement of the center of gravity, the greatest maximum trim incidence for the square cross-section missile is 24 deg, which coincides with the maximum incidence point of the aerodynamic data. For the circular cross-section baseline, because its center of gravity was placed in the same location as that of the square cross-section missile, the greatest maximum trim incidence is slightly different—greater by about 2.5 deg. Thus, a slight amount of extrapolation was required in that case in the narrow vicinities of these extremities.

In the orientations $\lambda = 45$, 135 deg, etc., although both maximum trim incidences are reduced, the square cross-section airframe fares relatively well. In the circular cross-section case the reduction is caused entirely by the modulating effect of the cruciform fins, which results in the overall diamond-like shape of the incidence contour. However, in the square case the fins-undeflected moments also reduce, as outlined earlier. Thus, the modulating effect of the fins is lessened, and this results, counterintuitively, in the incidence contour being more rounded.

Perhaps the starkest contrast that is evident from Fig. 5 is that of the maximum achievable nonrolling normal-force coefficient. In the control-frame pitch and yaw directions, the square cross-section airframe achieves an improvement of $\sim 40\%$ over the circular, even though the greatest achievable incidences are roughly the same in both cases. At some intermediate roll angles the improvement nears 100%, despite the fact that the rounded shape of the incidence contour of the square case does not scale uniformly to force. Actually, the force contour reverts to a diamond-like shape that is not very dissimilar from that of the circular cross-section baseline. The reason is evident from the fins-undeflected normal-force characteristics discussed earlier. As the planform area, with respect to the incidence orientation, reduces at the intermediate angles, so too does the force coefficient.

Had the approach instead been to make equal the cross-sectional areas, or had it involved matching the natural stability at low incidence, for example, by sizing the fins accordingly for each configuration, the trim capability might not have appeared so advantageous for the square configuration.

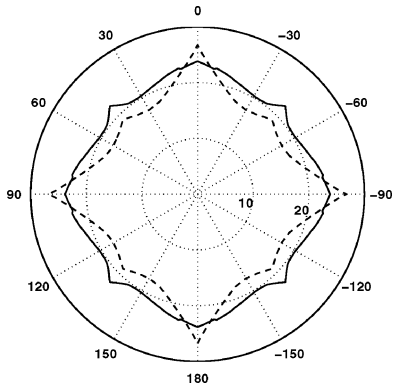

a) Total incidence (degrees)

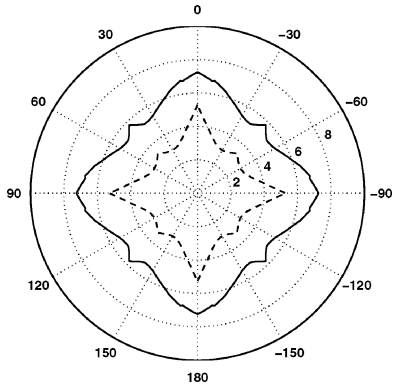

b) Nonrolling normal-force coefficient

Fig. 5 Maximum trim capability (dashed line, circular case; solid line, square cross-section case).

Uncontrolled Airframe

It is of interest to examine the natural stability of the airframes via the state space. Equations (2) and (3) are the state equations for the circular and square airframes at the particular trim case where the angles of attack and sideslip are both 11 deg, that is, total incidence of ~ 16 deg and aerodynamic roll angle of 45 deg. This condition is fairly close to the maximum trim capability of the circular. In the case of the circular airframe, the eigenvalues are ± 21, -0.37, and -0.35 ± 16j; in the square case they are -0.11, -0.59 ± 21j, and -0.42 ± 15j.

$$\begin{bmatrix} \dot{p} \\ \dot{q} \\ \dot{r} \\ \dot{v} \\ \dot{w} \end{bmatrix} = \begin{bmatrix} 0 & 0 & 0 & 1.5427 & -1.5427 \\ -0.0746 & 0 & 0 & -0.1680 & -0.1704 \\ -0.0746 & 0 & 0 & 0.1704 & 0.1680 \\ 146.1 & 0 & -720.7 & -0.5386 & -0.1624 \\ -146.1 & 720.7 & 0 & -0.1624 & -0.5386 \end{bmatrix} \times \begin{bmatrix} p \\ q \\ r \\ v \\ w \end{bmatrix} + B \begin{bmatrix} \xi \\ \eta \\ \varsigma \end{bmatrix} \tag{2}$$

$$\begin{bmatrix} \dot{p} \\ \dot{q} \\ \dot{r} \\ \dot{v} \\ \dot{w} \end{bmatrix} = \begin{bmatrix} 0 & 0 & 0 & 0.3099 & -0.3099 \\ -0.1040 & 0 & 0 & 0.2130 & -0.5091 \\ -0.1040 & 0 & 0 & 0.5091 & -0.2130 \\ 145.9 & 0 & -719.7 & -0.9533 & 0.1123 \\ -145.9 & 719.7 & 0 & 0.1123 & -0.9533 \end{bmatrix} \times \begin{bmatrix} p \\ q \\ r \\ v \\ w \end{bmatrix} + B \begin{bmatrix} \xi \\ \eta \\ \varsigma \end{bmatrix} \tag{3}$$

Cross coupling from the roll channel into incidence (v and w), and back the other way, is clearly evident from Eqs. (2) and (3). This cross coupling is the source of the fast unstable pole. This can be verified by changing the signs of the elements {1,4} and {1,5} of the A-matrix. The effect is to change the eigenvalues for the circular case to -0.37, -0.005 ± 21j, and -0.35 ± 16j and for the square case to 0.076, -0.49 ± 25j, and -0.42 ± 15j. These elements are proportional respectively to $\partial C_\ell / \partial \beta$ and $\partial C_\ell / \partial \alpha$, that is, they represent the slopes of the aerodynamic roll moment with incidence.

It turns out that the only regions of complete natural stability for the fully coupled circular airframe are around midincidence (i.e., roughly 8 to 14 deg of incidence) close to the control-frame pitch and yaw directions. For the fully coupled square airframe, in contrast, complete natural stability is achieved only at higher incidences (i.e., greater than about 17 deg of incidence) around the aerodynamic roll angles of ± 45 and ± 135 deg, where the circular airframe exhibits its fastest instability. These characteristics are closely related to

the fins-undeflected rolling moments discussed earlier and strongly influence the stability margins that are achieved with the autopilots.

It also turns out that the frequencies of the natural roll-mode instabilities tend to be higher in the circular case, compared with that of the square. The reason for this is not fully understood at the time of writing, but it might be because in a given trim condition the control deflections are generally greater in magnitude in the circular case.

Autopilot Robustness and Performance Requirements

Nichols Exclusion Regions

Consider the design objective of maximizing speed of response, subject to obtaining a minimum level of stability. This minimum level of stability is defined in terms of the elliptical-like Nichols exclusion region shown in Fig. 6. The region defines the uncertainties to be applied to all three feedback loops simultaneously. The closed-loop should remain stable in the presence of these multiple uncertainties.

The exclusion region is an approximation to the conventional ones used for fixed-wing military aircraft,[22,24] an example of which is also shown by the dotted line in Fig. 6. The use of straight edges is somewhat arbitrary and does not lend itself as well as an ellipse to automated analysis. The ellipse in Fig. 6 is defined by

$$\gamma = (1+\delta)/(1-\delta) \tag{4}$$

where δ is a complex number bounded in size by $|\delta| < c$ and c is a constant real number. Substituting $\delta = ce^{j\theta}$ (where $j = \sqrt{-1}$), and varying θ between 0 and 2π results in r tracing out an ellipse. By choosing the value of c appropriately, the ellipse can be made to approximate the conventional region based on straight edges. A value of $c = 0.25$ was used here, as this is commonly accepted as reasonable for multivariable analysis: it is equivalent to roughly 4.5 dB and 30 deg in the principal directions. The precise values selected for a production missile might differ slightly, depending on the assumed accuracies of the aerodynamic data, etc., that are available.

With the exclusion region parameterized in terms of a complex number, stability analysis can be turned into a μ-analysis[23] task. To understand the transformation into a form suitable for μ-analysis, consider the block diagram in Fig. 7. Writing down the relationship between e and u gives Eq. (4).

If there are three collective fin demands, namely, aileron, elevator, and rudder, then the block-diagram construction shown in Fig. 7 is added to each of these. Pulling the six δ blocks out of the resulting

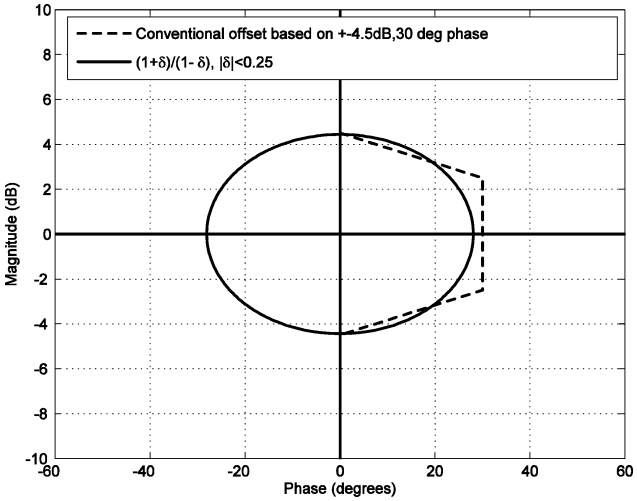

Fig. 6 Nichols exclusion regions.

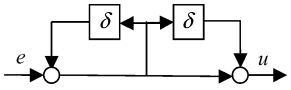

Fig. 7 Application of uncertainty to an actuator.

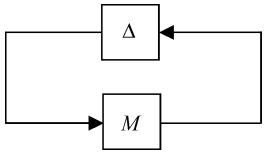

Fig. 8 Uncertainties pulled out from the interconnection structure M.

interconnection structure results in Fig. 8, in which M is the closed feedback loop of nominal airframe and autopilot, Δ is given by

$$\Delta = \begin{bmatrix} \delta_1 I_{2\times 2} & & \\ & \delta_2 I_{2\times 2} & \\ & & \delta_3 I_{2\times 2} \end{bmatrix}$$

and $I_{2\times 2}$ denotes the 2-by-2 identity matrix

$$\begin{bmatrix} 1 & 0 \\ 0 & 1 \end{bmatrix}$$

The permissible values of the δ_i define a set:

$$\mathbf{\Delta} = \{\text{diag}[\delta_1 I_{2\times 2} \quad \delta_2 I_{2\times 2} \quad \delta_3 I_{2\times 2}],\ |\delta_i| < 0.25\}$$

This is now in a format suitable for μ analysis, the uncertainty structure being three repeated complex blocks of size 2-by-2. The μ-analysis involves finding the so-called structured singular value of M, associated with $\mathbf{\Delta}$. The structured singular value is a frequency-dependent real scalar, defined[23] as

$$\mu := \begin{cases} 0 & \text{if} \quad \det[\mathrm{I} - M\Delta] \neq 0 \\ & \text{for any} \quad \Delta \in \mathbf{\Delta} \\ 1 \Big/ \min\limits_{\Delta \in \mathbf{\Delta}} \{\sigma_{\max}(\Delta) : \det[\mathrm{I} - M\Delta] = 0\} & \text{otherwise} \end{cases} \tag{5}$$

where $\sigma_{\max}(\Delta)$ is the maximum singular value of Δ. In turn, for the particular interconnection structure used here, the multivariable stability metric is defined as

$$\varepsilon_\mu := \min_{\omega}(1/\mu) \tag{6}$$

Given the structure of $\mathbf{\Delta}$ in this case, $|\delta_i| \leq 0.25\ \forall\, i$ is equivalent to $\varepsilon_\mu \geq 0.25$. It follows that the latter also represents the target multivariable stability margin, in that achieving $\varepsilon_\mu \geq 0.25$ implies that the uncertainty set defined in Fig. 6, when applied to all three effective actuators simultaneously, cannot destabilize the missile. Note that μ analysis is a linear frozen-point technique, so that any evaluation needs to be repeated at each node of a grid over the operating envelope.

Other Design Objectives

For each design, different stability metrics were used during the synthesis process, but all designs were finally assessed, in fully coupled form, using the μ-analysis tests just defined. The actual design objective during each design was to maximize speed of response, as measured by lateral acceleration rise time, subject to obtaining a minimum level of stability and satisfying certain high-frequency attenuation constraints.

To ensure some realism when designing the autopilot gains, it was assumed that the gain when breaking the feedback loop at the collective pitch and yaw demands must be less than -25 dB at 50 Hz; in the roll loop, the constraint was -25 dB at 75 Hz. These were imposed to limit any potential structural coupling problems via the inertial instruments. This approach was considered appropriate because the focus of the research was on basic aerodynamic effects rather than structural issues. In practice, the frequencies of the structural bending modes would be different in each airframe, possibly necessitating different high-frequency attenuation requirements and influencing the choice of actuator bandwidth.

Classical Three-Loop Autopilot

Background

A classical three-loop autopilot[13] was used to provide a baseline autopilot design for each airframe. It is by virtue of its simplicity and effectiveness that this methodology has seen widespread use in concept studies and real systems alike for a few decades. Nevertheless, it is a single-input-single-output technique with a comparatively restricted architecture, in terms of both individual loop shaping and cross terms, when considered against some relatively recent fully multivariable alternatives. This is particularly pertinent when evaluating the use of STT steering for noncircular airframes, which obviously involves handling simultaneously large values of angle of attack and sideslip, with potential for large cross coupling within the airframe. In practice, a classical architecture would usually be augmented with cross terms derived from the aerodynamics. For example, a decoupling matrix can be used to compensate for aerodynamic cross coupling that would otherwise arise from the collective roll, pitch, and yaw demands. The design of such cross terms can be problematic—for example, small errors in estimated aerodynamic roll angle or in the modeled aerodynamics can result in poor margins. The H_∞ design, described later, can be thought of as the limiting case of what could be achieved with careful design of cross terms.

The autopilot structure is shown in Fig. 9 and introduces three states, that is, one integrator per channel, and is based on a linear, frozen-point design methodology. At each flight condition of interest, a linear model of the airframe is derived, and the roll, pitch, and yaw autopilot channels are designed independently. In the final autopilot implementation, the gains are scheduled on Mach number and the angles attack and sideslip. Each autopilot channel was designed using third-order pole placement, ignoring the actuator and instrument states but including a second-order airframe representation. Note that all of the gains of a channel are synthesized at the same time: there is no need to synthesize the inner-loop gains first.

Application

The first step in the design procedure is to postulate some desired closed-loop pole locations for the controlled missile, as illustrated by Eq. (7) for the yaw channel; the roll and pitch channels are similar. The autopilot gains are then assigned in each channel by standard procedure.[25] The pole frequencies ideally should be as high as possible without violating stability and attenuation constraints; damping factors would typically be around 0.7.

$$(\tau_{yd}s + 1)\left[\left(1/\omega_{yd}^2\right)s^2 + \left(2\xi_{yd}/\omega_{yd}\right)s + 1\right] \tag{7}$$

Next, the design is evaluated with the actuator and instrument states included. This is done still in terms of pole locations and still one channel at once; the states of the other channels are ignored. Additionally, a test is performed to see if the attenuation constraint is being satisfied. If the damping moves too much, or the attenuation constraint is violated, then the desired pole locations are revised for the channel in question, and the process is repeated. Finally, the steady-state gains on the acceleration command inputs are calculated as functions of the gains already found and the airspeed.

H_∞ Autopilot

Background

Design using the H_∞ method covers a number of approaches. In this study, the H_∞ loop-shaping[14] methodology was applied. Figure 10 shows the closed-loop feedback structure. G is the missile airframe with the three collective fin demands as inputs and three gyros and two accelerometers as outputs. W_1 and W_2 are weighting matrices chosen by the designer using conventional loop-shaping objectives, that is, sufficient open-loop gain at low frequency for disturbance rejection, roll-off at high frequency for attenuation of noise and structural flexure, and suitable stability margins around gain crossover. Given W_1 and W_2, the normalized coprime factorization of the shaped plant $G_s = W_2 G W_1$ is defined by[14]

$$G_s = M^{-1}N$$

where M and N are the so-called coprime factors of G_s and satisfy the normalization condition:

$$[M \quad N]\begin{bmatrix} M^* \\ N^* \end{bmatrix} = MM^* + NN^* = I$$

where the superscript $*$ indicates the complex conjugate transpose. Note that M here has a different meaning to that used earlier in the definition of μ.

This factorization is then used as a framework in which to define uncertainty on the shaped plant G_s by introducing additive uncertainty on each of the factors:

$$G_{s_\Delta} = (M + \Delta_M)^{-1}(N + \Delta_N)$$

There is evidence of this being a good representation of typical plant uncertainty from a number of sources, including application

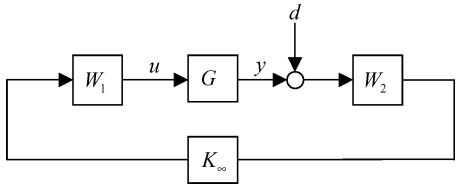

Fig. 10 H_∞ loop-shaping autopilot structure.

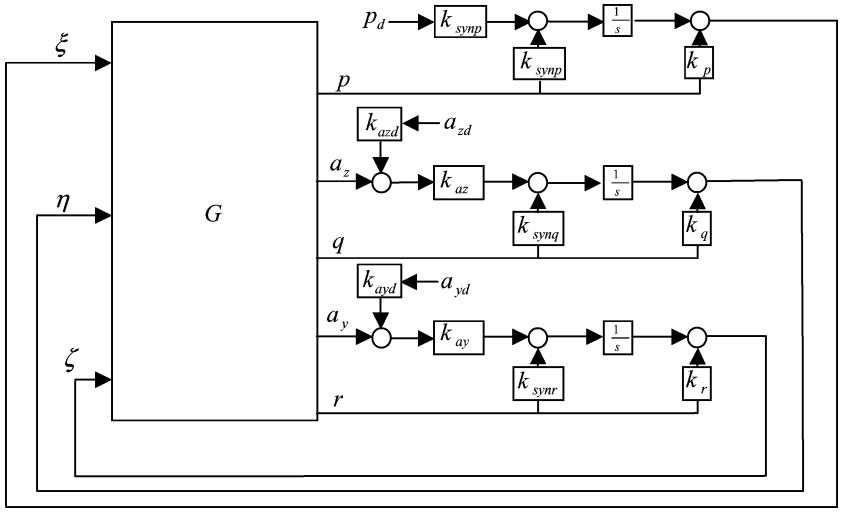

Fig. 9 Three-loop autopilot structure.

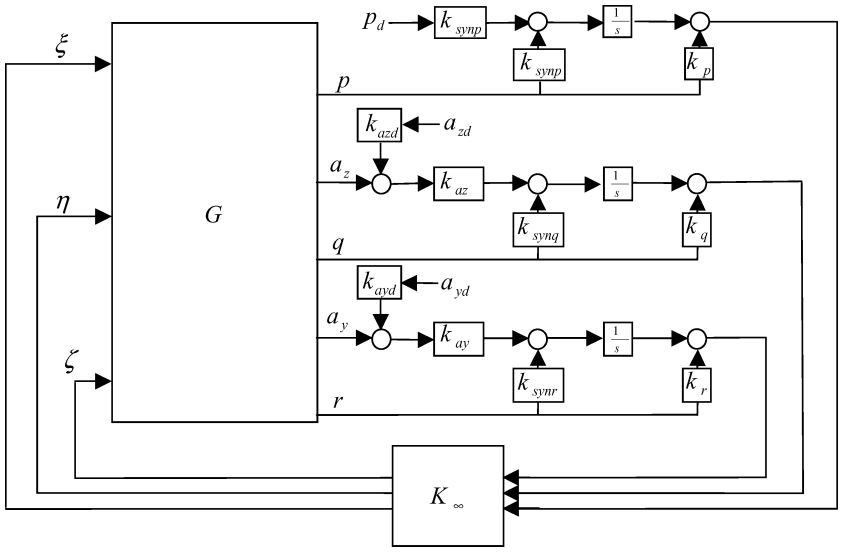

Fig. 11 Three-loop autopilot structure with H_∞ loop-shaping compensator.

to experimental flight control[16,18] and links to the gap metric and interpretation in terms of the Riemann sphere.[26] More recently it has been shown that this type of uncertainty is equivalent to the application of offsets defined by Eq. (4) to all actuators and sensors simultaneously.[27] Hence, it might be expected that obtaining closed-loop robustness to normalized coprime-factor uncertainty would provide some level of robustness in the case where all of the uncertainty is defined to be at the actuators. In practice, this will be true provided that the input weighting matrix W_1 is diagonal.

It has been shown[14] that the controller that maximizes the robustness to uncertainty on the normalized coprime factors is given by solving

$$\min_{K_\infty} \left\| \begin{bmatrix} I \\ K_\infty \end{bmatrix} (I - G_s K_\infty)^{-1} M^{-1} \right\|_\infty = \frac{1}{\varepsilon_{\text{ncf}}} \tag{8}$$

This optimization can be solved using solvers[28] that are implemented in the MATLAB Mutools toolbox.

Application

Figure 11 shows the architecture used in the study. The three-loop autopilot is taken to be the weight W_2, and W_1 is set to the identity matrix. Hence the H_∞ compensator is used to fine tune the loop shapes at the actuators, adding cross terms as necessary to achieve good robustness to normalised coprime-factor uncertainty.

The autopilot introduces 21 states in addition to the three for the weight W_2, resulting from the classical design, and, like the classical, is based on a linear, frozen-point design methodology. At each flight condition of interest, a full-order linear model of the airframe is derived, and the roll, pitch, and yaw autopilot channels are all designed simultaneously. In the final autopilot implementation the gains are scheduled on Mach number and the angles attack and sideslip. The controller K_∞ is implemented in an observer form as originally deployed on a fixed-wing application,[15] thereby facilitating gain scheduling with operating point. Model-order reduction of the 21-state compensator to 10 states was found to be possible with less than 1% degradation in stability margin. This is approximately one state per input-output pair of the three-input three-output compensator, which is not excessive. However, there is no guarantee that the model-reduced controllers can still be gain scheduled by interpolating the state-space matrices.[16] The NDI autopilot described next would arguably be simpler to implement in practice.

NDI Autopilot

Background

The NDI method inverts the system dynamics up to some specified frequency, that is, the desired closed-loop bandwidth. An advantage of the NDI approach is that no separate gain scheduling is required, and hence its implementation is, in principle, more straightforward. It also incorporates knowledge of the nonlinear system into the design, and hence it might be expected that better performance could be achieved. A disadvantage is that it does not directly address robust stability, and hence the stability-performance tradeoff is not easily made. One approach to mitigate this has been proposed,[29] whereby the NDI method is combined with a simple lead-lag inner-loop compensation scheme designed with the aid of coprime-factor-based stability analysis. Here we apply NDI without this fine tuning, but use ε_μ to help select suitable closed-loop dynamics.

The missile airframe equations can be written in the following form:

$$\dot{x} = F(x) + G(x, u) \tag{9}$$

For NDI, the usual assumption is that the equations are linear in the control, that is,

$$\dot{x} = F(x) + G(x)u \tag{10}$$

In many papers this is not an issue, typically because BTT steering is presumed and a design objective is to keep sideslip close to zero. This is not the case here: the control moments are nonlinear functions of both the states and the controls, and relatively large angles of attack and sideslip can be experienced simultaneously. In this situation various options present themselves for obtaining the controls, one being to assume small perturbations about trim, and another to invert the control moments directly. Both of these options were considered, but the results presented here are for the latter, which obtained the better robustness. Expanding on the specific terms in x and u on which the control term depends gives

$$\dot{x} = F(x) + G(\sigma, \lambda, \varsigma, \eta, \xi) \tag{11}$$

Hence, inversion involves finding and implementing a five-dimensional table with desired moments (L, M, N) and current incidence values as inputs, and the roll, pitch, and yaw collective fin demands as outputs. Note that inversion does not result in equations that are linear in the control, but this does not prevent the assignment of the closed-loop dynamics to some desired set of values.

Application

Figure 12 shows the autopilot architecture that was used in this study. The inner loop contains an NDI controller for roll, pitch, and yaw control. The resulting closed inner-loop response can be made first order,[20] as was done here. For the outer acceleration loop, the timescale separation approach[21] was tried, but it was found that an outer classical architecture could provide faster acceleration tracking. The outer-loop gains were set to achieve desired speed

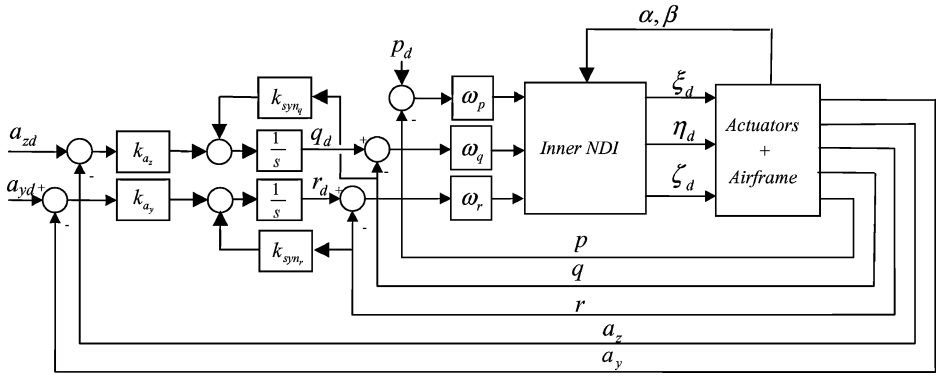

Fig. 12 Inner-loop NDI autopilot plus classical outer loop.

of response and less than 2% overshoot. The desired inner-loop bandwidths ω_p, ω_q, and ω_r were made as fast as possible while respecting the required stability margin ε_μ. The design procedure comprised the following: 1) postulate values for ω_p, ω_q, and ω_r; 2) design the outer loop to achieve desired rise time and overshoot; and 3) calculate ε_μ 4) if ε_μ is too small, or if the high-frequency attenuation constraints are violated, revise the values for ω_p, ω_q, and ω_r and/or the desired outer-loop rise time, and repeat the procedure.

Pushing the desired inner-loop bandwidths too high results in poor robustness caused by the cumulative phase lag of actuators, sensors, and short-period mode. Conversely, making them too low fails to stabilize the short-period and unstable roll modes. Similarly, too aggressive an acceleration response adversely affects stability margins.

The inner-loop NDI is based on the following moment equations, taken about the center of gravity:

$$J\dot{\Omega} + \Omega^{\wedge} J\Omega = (x_{\text{aero}} - x_{\text{cg}})^{\wedge} S_{\text{ref}} Q \begin{bmatrix} C_{X0} \\ C_{Y0} \\ C_{Z0} \end{bmatrix} + S_{\text{ref}} DQ \begin{bmatrix} C_{L0} \\ C_{M0} \\ C_{N0} \end{bmatrix} + S_{\text{ref}} DQ \begin{bmatrix} \Delta C_\xi \\ \Delta C_\eta \\ \Delta C_\varsigma \end{bmatrix} \tag{12}$$

Assigning the desired closed-loop dynamics with

$$\dot{\Omega} = \begin{bmatrix} \omega_p(p_d - p) \\ \omega_q(q_d - q) \\ \omega_r(r_d - r) \end{bmatrix}$$

and rearranging gives the desired fin moment coefficients as

$$\begin{bmatrix} \Delta C_\xi \\ \Delta C_\eta \\ \Delta C_\varsigma \end{bmatrix} = \frac{1}{S_{\text{ref}} DQ} \left\{ J \begin{bmatrix} \omega_p(p_d - p) \\ \omega_q(q_d - q) \\ \omega_r(r_d - r) \end{bmatrix} + \Omega^{\wedge} J\Omega \right\} - \frac{(x_{\text{aero}} - x_{\text{cg}})}{D} \wedge \begin{bmatrix} C_{X0} \\ C_{Y0} \\ C_{Z0} \end{bmatrix} - \begin{bmatrix} C_{L0} \\ C_{M0} \\ C_{N0} \end{bmatrix} \tag{13}$$

These desired moments are converted into collective fin demands by off-line inversion of the aerodynamics and are implemented as the five-dimensional look-up table, discussed earlier.

Robustness Analysis

The robustness analysis results, in which robustness is indicated by ε_μ, are presented in Fig. 13. As expected, the target multivariable stability margin is satisfied at lower incidences by all of the designs on both missiles. As the incidence magnitude increases, so the mean level of ε_μ reduces and undulation with incidence orientation becomes more pronounced, reflecting the increasing influence of cross coupling and the stability characteristics of the roll mode. These trends tend to be more prominent with the square cross-section missile, consistent with the relatively higher levels of cross coupling in that case.

Only the H_∞ designs meet the criterion of $\varepsilon_\mu > 0.25$, but the NDI designs are close to achieving it. The classical three-loop designs achieve lower ε_μ than the other designs at low incidences, but still essentially meet the target multivariable stability margin for all incidences up to about 15 deg. Given that the peak values of ε_μ are little more than 0.25 in the classical cases however, it is perhaps not surprising that these designs fail by a significant amount to meet the target margin in the worst-case higher incidence conditions. The isolated-channel gain and phase margins of the classical three-loop designs generally satisfy 6 dB and 30 deg.

The extent to which the mean level of ε_μ reduces as incidence magnitude increases can be partly attributed to the compensator order that is afforded by the design methodology. The NDI and classical three-loop methodologies produce designs of restricted order, and so the amount of shaping that can be added around gain crossover to counter the lag of the actuators, etc., while stabilizing the airframe and satisfying design attenuation constraints, is limited. The H_∞ methodology, in contrast, has much greater freedom in this regard.

The undulation with aerodynamic roll angle does not always follow what might at first be considered as a consistent pattern. Investigations indicated that for the classical design ε_μ tends to be dominated by the robustness of the roll loop, which is itself correlated with the natural stability characteristics of the airframe roll mode. Accordingly, with the classical design it is no coincidence that the worst-case ε_μ occurs at, or close to, those aerodynamic roll angles where the airframe roll mode is fastest unstable. The undulation is shifted in phase between the two missiles in accordance with the fins-undeflected aerodynamic roll characteristics. For the H_∞ and NDI designs the roll loop does not always dominate over the pitch and yaw loops in contributing to ε_μ. This is thought to be because of the cross terms that are afforded by these multivariable methods, and, in the H_∞ case, by the much higher-order compensation.

The best are the H_∞ designs, which are shown to meet the robustness criterion at all of the incidences considered. These results, in particular, suggest that the square cross-section missile is adequately controllable over the incidence envelope under examination, that is, up to 24 deg all around the body. More generally, they add confidence that a realistic square cross-section missile with control fins at the rear should be controllable to similar moderate incidence levels.

The action of the H_∞ designs of this study was effectively to fine tune the classical three-loop autopilots in automated fashion by introducing high-order primary and cross-channel compensation. It is therefore reasonable to infer that the stability of the classical three-loop autopilots could be improved by classical means, adding additional shaping, explicit cross-compensation paths, etc., to the standard architecture—as is commonly done in practice. Additionally, or alternatively, higher bandwidth actuators could be employed, provided structural characteristics permit.

Over the incidence range considered, the square airframe was found not to pose a significantly harder design problem than that

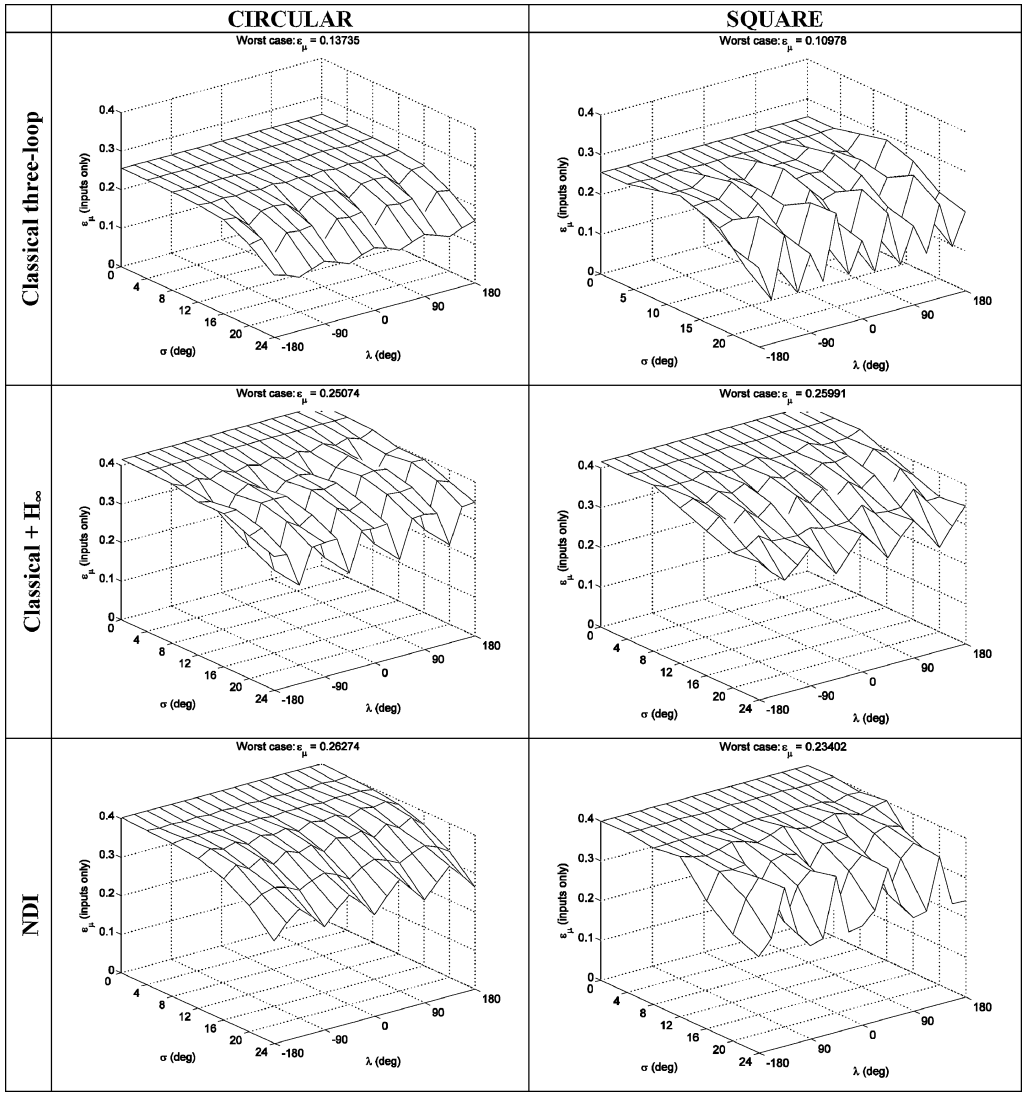

Fig. 13 Robustness results as measured by ε_μ.

of the circular cross-section baseline. One of the reasons for this is considered to be that the frequencies of natural roll-mode instability are actually somewhat lower in the square case, giving wider separation from the assumed actuator mode, thereby making phase margin easier to obtain. In respect of the H_∞ designs, this is thought to be the reason for the worst-case value of ε_μ being slightly better in the square case than with the circular cross-section baseline.

Steering Laws

The study considered a number of steering laws, largely inspired by Kaufmann.[9] Three of these, namely, STT, STT-45BTT, and 180BTT, are presented in this paper. The first and last represent, in some senses, the two extremes and are the most commonly used in air vehicles. STT is the traditional law for circular cross-section missiles and so was regarded as the baseline steering law of the study. STT-45BTT is presented because it gives the best results, according to the metrics used, of all of the steering laws considered.

STT

The aim with this law is to accomplish maneuvers without deliberate rolling. The version adopted is based on the feedback of integral body roll rate, which is better behaved than Euler roll angle and more closely related to the roll-channel dynamics of the autopilot:

$$p_d = k_{\phi e}\left(\phi_c - \int_{t_0}^{t} p\,\mathrm{d}\tau\right), \qquad a_{yd} = a_{yc}, \qquad a_{zd} = a_{zc}$$

STT-45BTT

By combining the actions of STT and 45BTT, this law offers the fast reaction time of STT and the high maximum trim capability of BTT. Hence, any maneuver orientation is permitted in the short term, but the long-term aim is to keep maneuvers close to either the pitch plane or the yaw plane of the missile. The 45BTT steering permits positive and negative angles of either attack or sideslip—hence the need to roll through commanded changes in roll angle of up to ±45 deg.

$$p_d = k_{\phi e}\left(\phi_{e_1} + \phi_{e_2}\right)$$

$$\phi_{e_1} = [(-a_{zc} \geq |a_{yc}|) - (a_{zc} \geq |a_{yc}|)] \cdot a_{yc}/(a_{\text{bias}} + |a_{zc}|)$$

$$\phi_{e_2} = [(a_{yc} > |a_{zc}|) - (-a_{yc} > |a_{zc}|)] \cdot a_{zc}/(a_{\text{bias}} + |a_{yc}|)$$

$$a_{yd} = a_{yc}, \qquad a_{zd} = a_{zc}$$

180BTT

This law implements BTT with positive angles of attack only—hence the need to roll through commanded changes in roll angle of up to ±180 deg. The aim is to keep maneuvers close to the pitch upper-half plane of the missile. Because of the need to roll through larger roll angles, this law tends to involve higher roll rates, over longer periods of time, than 45BTT. Accordingly, the magnitude of any roll-rate limit becomes an important effect.

$$p_d = k_{\phi e}\left(\phi_{e_1} + \phi_{e_2}\right), \qquad \phi_{e_1} = \frac{a_{yc}}{a_{\text{bias}} + (a_{zc} < 0) \cdot |a_{zc}|}$$

$$\phi_{e_2} = [(a_{yc} \geq 0) - (a_{yc} < 0)] \cdot \frac{(a_{zc} > 0) \cdot a_{zc}}{a_{\text{bias}} + (a_{zc} < 0) \cdot |a_{zc}|}$$

$$a_{yd} = 0, \qquad a_{zd} = (a_{zc} < 0) \cdot a_{zc}$$

In the preceding, ϕ_c (=0); a_{yc} and a_{zc} are the roll angle and acceleration commands prior to the steering function; and p_d, a_{yd}, and a_{zd} are the roll rate and modified acceleration commands resulting from it. These quantities are taken with respect to the control frame, and the accelerations are gravity compensated, that is, they are the components of total acceleration minus gravity. The $k_{\phi e}$ is a gain, abias is a positive constant inserted to avoid the possibility of division by zero, and the notation $(a > b)$, etc., is interpreted as unity if true, zero otherwise.

Effective Time Constant

The lag that is introduced into the guidance loop by the autopilot and steering functions can be encapsulated by a single effective time constant. With a circular cross-section missile under STT steering, this time constant can be adequately defined as the time taken to reach 63% of the magnitude of an acceleration step command. At a given operating condition, it is not unreasonable to expect its value to be roughly the same for any maneuver direction around the body. This is consistent with the definition of time constant for a simple lag, although nonlinearities can mean that the value observed is dependent on the magnitude of the command itself.

When the steering law contains an element of BTT, it becomes necessary to extend the definition of the effective time constant. A possibility is to take the time taken to reach 63% of the magnitude of an acceleration step command *and* 63% of the direction of that command.[9] A drawback with this is that steering laws cannot easily be compared in a consistent manner. Hence, a new definition was adopted: the time taken to get to within a circle, centered on the acceleration step command vector, of radius 37% of the command magnitude. In other words, the effective time constant is the elapsed time taken to satisfy

$$1 - \sqrt{\frac{(a_y - a_{yc})^2 + (a_z - a_{zc})^2}{a_{yc}^2 + a_{zc}^2}} = 0.63$$

where $\{a_{yc}, a_{zc}\}$ and $\{a_y, a_z\}$ are, respectively, the commanded and actual accelerations with respect to the control frame. This definition makes the effective time constant dependent on the angle through which the missile has to roll. By implication, it is also dependent on the roll-rate design limit itself.

The effective time constants for small-magnitude commands and the specified roll-rate limit are compared in Fig. 14. The smallest time constants, as well as the most uniform with maneuver direction, are obtained with STT and STT-45BTT, which appear to be almost as good. In worst-case maneuver directions, 180BTT steering is between four and five times slower. This is not unexpected, as the roll-rate limit comes into play. Note that the H_∞ autopilots are faster than the others in worst-case maneuver directions, reflecting

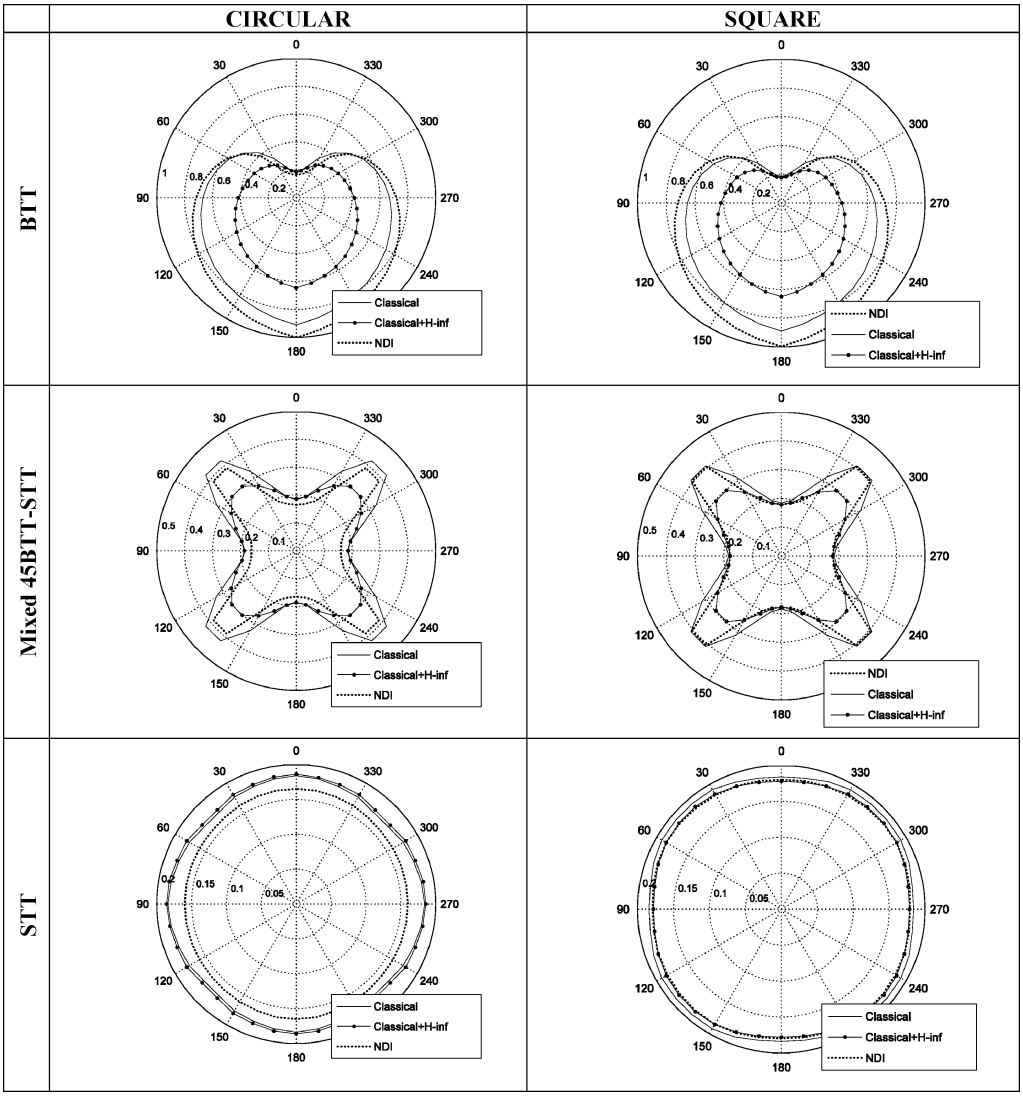

Fig. 14 Effective time constant plots.

the fact that the H_∞ compensator increases roll bandwidth in order to improve the multivariable robustness margin. Any particular steering law gives very similar results whether applied to the circular or the square cross-section missile. Of course, some basic shape characteristics would be similar because both missiles have four planes of symmetry. In practice, exposed lugs, etc., would distort some of the symmetry that is seen here in respect of the STT and STT-45BTT steering laws.

Maneuver Reach Capability

Maneuver reach capability is used here as an indicator of maneuverability. It can be interpreted as the maximum distance that it is possible to reach in a direction perpendicular to the current flight path, or it can be interpreted as an entire reachable zone ahead of the missile. Whether it is more appropriate to consider reachable distances or entire zones arguably depends on the application and particular scenario, as well as the nature of the uncertainty that is associated with the missile-target states. With either interpretation, this metric combines both the maximum trim capability of the airframe and the effective time constant of the autopilot and steering. Arguably therefore, the metric relates more closely to miss distance than do the other metrics in isolation.

Obviously, the distance that can be reached perpendicular to the current flight path is dependent on the flight duration ahead of the current time. For flight durations that are at least an order of magnitude greater than the effective time constant, the metric is completely dominated by the maximum trim capability; otherwise, as flight durations reduce, the influence of the effective time constant becomes increasingly significant.

The results presented here correspond to the situation in which there is no thrust, thereby ensuring that there is no bias caused by thrust contribution to lift. The speed is decaying naturally from a starting condition of Mach 2.5, 10 km altitude, and zero incidence: because the available aerodynamic data were for Mach 2.5 only, it was necessary to assume that the nondimensional aerodynamic characteristics did not change with Mach. Because of its higher drag at maximum trim incidence—the drag at this incidence arises almost entirely from its induced drag component—the square configuration loses speed more rapidly than does the circular. Nevertheless, provided the aerodynamic coefficients do not change significantly with Mach and provided there is no maneuver limiting, the loss of speed has little effect on the maneuver reach capability. This is because the lateral force required for a given turn radius and the available aerodynamic lift are then both directly proportional to the square of the speed. The square configuration takes longer to achieve a given downrange, but the effect of this difference is fairly small at the downranges considered.

Three sets of reach boundaries, normalized by the reach capability of the circular configuration in the 0-deg maneuver direction, are plotted for each airframe in Fig. 15. The 0-deg direction is pitch-up with the fins orientated in a cross and the square body in a diamond. The results were obtained using the classical three-loop autopilot and with the 400-deg/s roll-rate limit, but otherwise

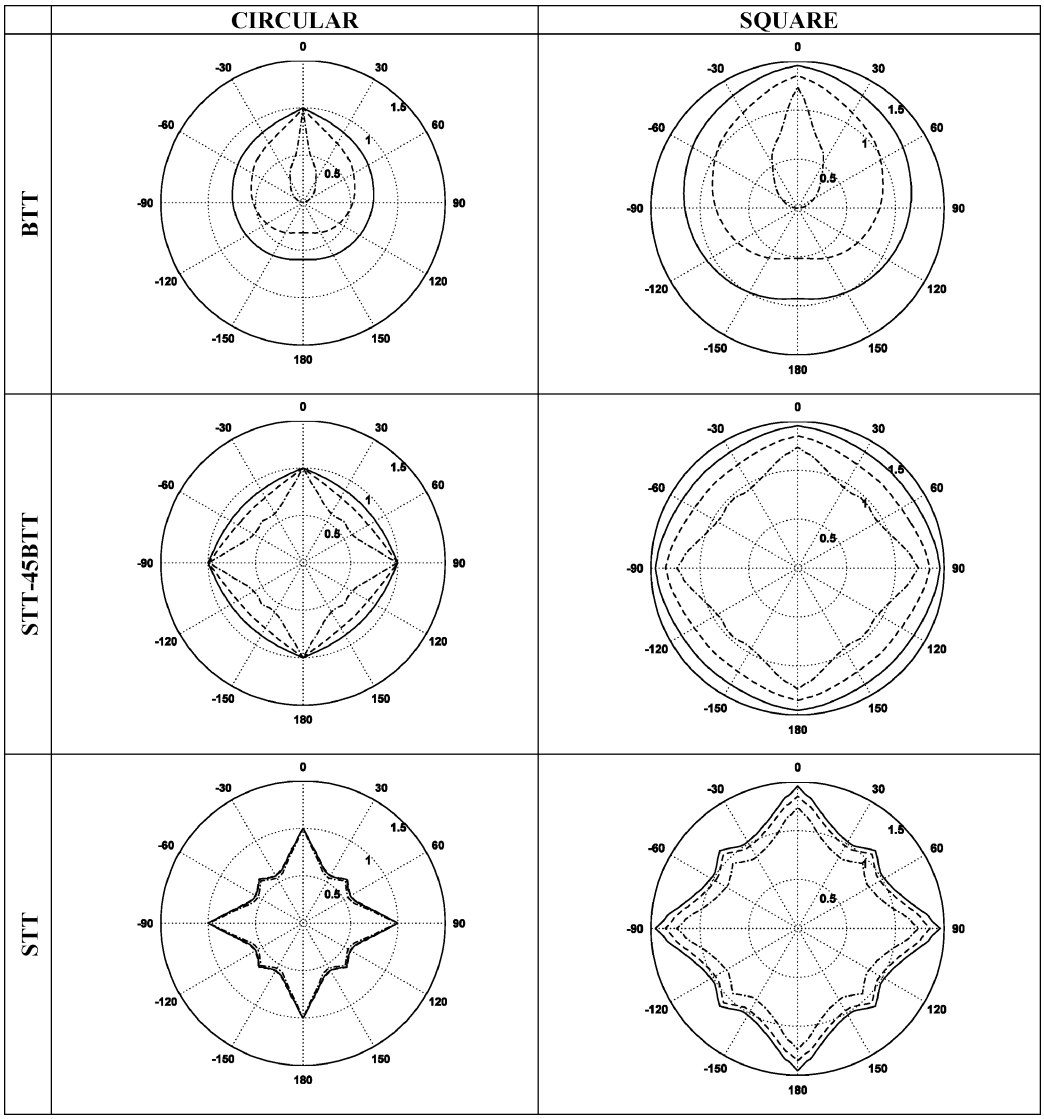

Fig. 15 Normalized maneuver reach for the square and circular airframes: ——, 2 km; – – –, 1 km; and ·–·–, 300 m range to go.

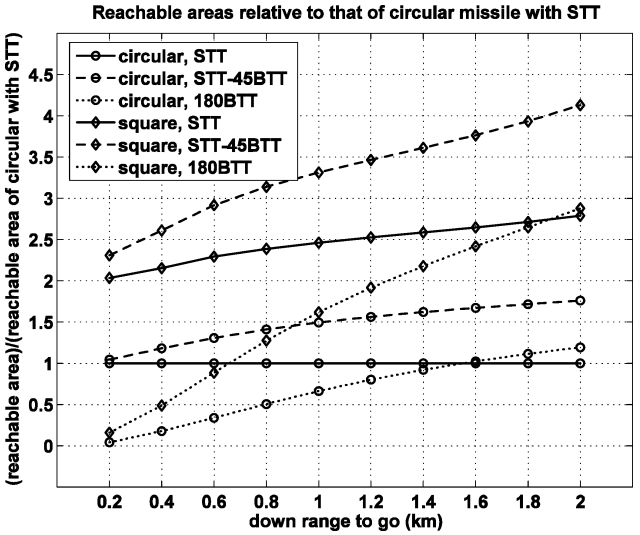

Fig. 16 Comparison of reachable areas for various steering laws as a function of downrange to go.

without any rate limiting, whether on acceleration commands or within the autopilot or actuators. Each set is for a particular steering law—STT, STT-45BTT, or 180BTT—and considers the same three downranges: 2 km, 1 km, and 300 m. At the given speed, these ranges correspond to durations of approximately 3.5, 1.5, and 0.4 s, respectively. The square cross-section missile clearly has much greater maneuver reach capability, that is, approaching double that of the circular cross-section baseline in some maneuver directions at 2 km downrange. These are expected characteristics given the respective maximum trim capabilities, illustrated in Fig. 5.

Some of the plots in Fig. 15 clearly show the evolving influences of trim and time constant. With STT steering, the shapes of the normalized reach boundaries are seen not to change significantly with downrange: the effective time constant does have a bearing, particularly at shorter downrange, but the effect is almost independent of maneuver direction. Now take the 180BTT case: 2 km of downrange represents over 15 effective time constants in the 0-deg maneuver direction, but only about four effective time constants when the maneuver direction is ± 180 deg. As a result, the reach capability in the latter case, in terms of radial extent, is only $\sim 60\%$ of that of the former. At 300 m of downrange, there is no capability at all in any lateral or downwards directions, which is not surprising, as the effective time constant is greater than the flight duration.

Capability in terms of reachable area, relative to that of the circular cross-section missile operating under STT steering, is shown in Fig. 16 and serves to reinforce the earlier findings. Clearly, the best performance, by this metric, is obtained with STT-45BTT steering (though it must be remembered that roll rates induced by BTT steering can have deleterious effects on other elements of the guidance loop). If the choice of steering were restricted to STT and 180BTT, these results would suggest that the ranges at which to switch from the latter to the former would be ~ 1.6 km in the case of the circular cross-section missile and ~ 1.9 km for the square configuration.

The extent to which the maneuver reach capability of the square configuration is greater than that of the circular stems largely from the differences in the trim capabilities. As stated for the latter, the advantage might not have appeared quite so large had comparison been made using airframes of the same cross-sectional area or of similar natural stability at low incidence.

Conclusions

A square cross-section supersonic rocket-propelled missile has been investigated in terms of control, stability, and performance metrics, taking cognizance of the desire for maneuverability. Comparisons were made, whenever possible, with an equivalent circular cross-section baseline. The square configuration was effectively evolved from the baseline, the only essential differences being the cross section of the body and the influence of this on the shape of the nose; the width of the side of the square body was made equal to the diameter of the circular. These are wingless configurations with rear fins, and because the fins in the square case are mounted in the middle of the flat sides, it was possible to have identical fin shape and arrangement in both cases. The two missiles were also assumed to have the same center-of-gravity location and mass. The aerodynamic data were provided to some extent by experiment, but mainly by CFD prediction. The predicted data were for one Mach number, all-round-the-body incidences up to moderate level and several control deflections.

Fundamental aims were to assess the degree to which a square cross-section airframe can be controlled and to explore ways in which the aerodynamics can be exploited to maximize performance attributes. To these ends, three autopilot designs, based on classical three-loop, NDI, and H_∞ loop-shaping architectures, were synthesized and compared for each missile. Each of the designs was analyzed in terms of a multivariable robustness metric based on μ analysis. Additionally, three steering laws, namely, STT, STT-45BTT, and 180BTT, and a new metric for missile responsiveness, that is, for the missile effective time constant, were defined. The metric facilitates comparison of the combined effects of the autopilot and steering functions. Other metrics have also been used to assess performance, including the maximum trim and maneuver reach capabilities.

The key findings are as follows:

1) The square cross-section missile of the study should be controllable, with sufficient stability margins, at least up to the incidences considered, that is, up to 24 deg all around the body. This has been predicted by the application of H_∞ loop shaping—a multivariable autopilot design methodology. Various forms of steering, including ones involving STT, where there can be simultaneously large angles of attack and sideslip, appear to be feasible.

2) Notwithstanding, robust autopilot design proved more difficult at higher incidences, where none of the designs exceeded the target stability margin with much to spare. The situation is mitigated by the fact that the general reduction of margin with incidence afflicts both the square and circular cross-section missiles to a similar degree. Nevertheless, with the square cross-section missile the classical three-loop and NDI autopilots exhibit a greater undulation of margin with aerodynamic roll angle. This might be indicative of how autopilot design difficulty would increase at incidences higher than those hitherto considered.

3) The controlled maneuverability of the square cross-section missile of the study is predicted to be substantially greater than that of the circular cross-section baseline. There appears to be a minimum of $\sim 40\%$ more trim normal force capability in the pitch and yaw directions, that is, when the square body is in the diamond orientation; the figure is significantly higher in some intermediate orientations. In terms of maneuver reach capability, there is predicted to be a similar improvement in radial extent. Of the steering laws considered, STT-45BTT appears to give the best results as far as maneuverability is concerned.

On the preceding findings some cautionary remarks are in order. Arguably, a systems approach was adopted in selecting the widths of the two airframes such that the square body just fitted around that of the circular. Ignoring structural practicalities, this allowed the same internal configuration, that is, the internal configuration of the circular missile, to be assumed for both, hence also the same mass. It also resulted, however, in the square configuration having a larger cross-sectional area and a nose with a greater apex angle, which in turn resulted in a significant increase in axial force and contributed to a reduction in static stability at low incidence.[11] This reduction in stability could give rise to additional concerns if it were to pertain at release speeds; nevertheless, it might favor the square in terms of maneuverability. If the cross-sectional areas had been made the same, giving the square configuration a higher fineness ratio, or if the natural stability levels had been matched at low incidence by accordingly adjusting one of the configurations, the maneuverability results might not have favored the square cross section to the same

extent. For practical reasons, the aerodynamic data sets for the two airframes were not generated in precisely the same fashion: the data set for the square was essentially all CFD based, whereas that for the circular was composed of both measured and CFD prediction. In respect of the square airframe, tunnel test results[11] indicated that rolling moment and nonrolling side-force and yawing-moment coefficients were underpredicted in the worst case, that is, at maximum incidence in the 22.5-deg aerodynamic roll orientation, by between $\sim$10 and $\sim$25%. The potential effects of such are not taken into account in the results of this paper.

The work has provided additional insight into the autopilot design methods. For both airframes, the standard three-loop autopilot does not provide the necessary architecture in terms of high-order shaping or cross-term compensation. Accordingly, stability margins are necessarily compromised at higher incidence levels. The NDI methodology, despite including the nonlinear dynamics in the design process, performed marginally worse, in the context of the square cross-section missile, than did the H_∞ approach. A more systematic means of inverting the control moments and of manipulating the high-frequency behavior of the NDI autopilot is required.

Consideration has thus far been confined to a single Mach number and incidences that are no more than moderate in level. To explore fully the potential of a square cross-section missile in terms in controllability and maneuverability, an investigation over a wider operating envelope is required. In particular, much higher incidences—at least up to 40 deg, possibly as high as 60 deg—should ideally be considered, along with correspondingly greater fin deflections. Cognizance should be taken of both single and combined deflections, for example, elevator as well as rudder, in case there are mutual interferences, particularly at the higher incidences. The structural design implications of realizing agile square cross-section missiles need to be assessed and incorporated into future autopilot design studies. For example, a certain amount of corner rounding might have to be considered. Simple design attenuation constraints have been used hitherto in anticipation of the more refined structural filtering that would ultimately be required.

There is much scope for investigating other variations in the square cross-section configuration. Boat tailing and alternative nose shapes should be explored. The effects of reducing the span of the side-mounted fin to just half the width of the side of the square body should be considered. If this were feasible it would enable the fin to be stowed folded, by a single hinge arrangement, along the flat side of the body, without overlapping the corner. Finally, the relative merits should be investigated of side-vs-corner mounting positions for the fins.

Acknowledgments

This work was funded by the Energy, Guidance, and Control Domain of the United Kingdom (UK) MOD Corporate Research Programme. The authors would also like to thank Trevor Birch, of the UK MOD Defence Scientific and Technical Labs, for his advice on aerodynamics; Dave Lee of QinetiQ Farnborough, for his advice on control and performance; and aerodynamics staff of QinetiQ Bedford, who made available the aerodynamic data.

References

[1]Jorgensen, L. H., "Inclined Bodies of Various Cross Sections at Supersonic Speeds," NASA Memo 10-3-58A, Nov. 1958.

[2]McGehee, R. M., and Emmert, R. I., "Bank-to-Turn (BTT) Autopilot Technology," *Proceedings of the IEEE National Aerospace and Electronics Conference*, Vol. 2, IEEE Publications, Piscataway, NJ, 1978, pp. 688–696.

[3]Huber, A., Ford, K., Mook, R., and Woods, D., "Have Dash II: Development Test and Evaluation of an Advanced Air-to-Air Missile Concept," *Proceedings of 36th Symposium of Experimental Test Pilots*, 1992, pp. 139–158.

[4]Agrell, J., Hamnér, O., and Jonsson, B., "Aerodynamics of Missiles with Triangular Cross-Sections," *Proceedings of the 21st ICAS Congress*, AIAA, Reston, VA, 1998.

[5]Lee, K. L., Langehough, M. A., and Chamberlain, R. A., "Modern Control Bank-to-Turn Autopilot for Have Dash II Missile," *Proceedings of 1st IEEE Conference on Control Applications*, Vol. 1, Sept. 1992, pp. 214–219.

[6]Schumacher, C., and Khargonekar, P., "Missile Autopilot Design Using H_∞ Control with Gain Scheduling and Dynamic Inversion," *Journal of Guidance, Control, and Dynamics*, Vol. 21, No. 2, 1998, pp. 234–243.

[7]Halsey, K. M., "Nested Feedback Systems," Ph.D. Dissertation, Dept. of Engineering, Univ. of Cambridge, England, UK, Sept. 2002.

[8]Arrow, A., "Status and Concerns for Bank-to-Turn Control of Tactical Missiles,"*Journal of Guidance, Control, and Dynamics*, Vol. 8, No. 2, 1985, pp. 267–274.

[9]Kaufmann, W. A., "Flight Control Design Issues in Bank-to-Turn Missiles," *AGARD Lecture Series in Missile Interceptor Guidance System Technology*, No. 173, AGARD, Neuilly-sur-Seine, France, 1990, pp. 2-1–2-18.

[10]Cleminson, J. R., Lee, D. W., Hodgson, J. A., and Hyde, R. A., "Selected Control and Steering Issues for Non-Axisymmetric Missiles," *Proceedings of the Royal Aeronautical Society Missile Aerodynamics Conference*, Royal Aeronautical Society, London, 1999, pp. 2-1–2-18.

[11]Birch, T., and Cleminson, J. R., "Aerodynamic Characteristics of a Square Cross-Section Missile Configuration," AIAA 22nd Applied Aerodynamics Conf., AIAA Paper 2004-5451, 2004.

[12]Wilcox, F. J., Jr., Birch, T. J., and Allen, J. M., "Force, Surface Pressure and Flowfield Measurements on a Slender Missile Configuration with Square Cross-Section at Supersonic Speeds," *Proceedings of AIAA 22nd Applied Aerodynamics Conference*, AIAA, Reston, VA, 2004.

[13]Nesline, F. W., and Nesline, M. L., "How Autopilots Constrain the Aerodynamic Design of Homing Missiles," *Proceedings of the American Control Conference*, 1984, pp. 716–730.

[14]Glover, K., and McFarlane, D. C., "Robust Stbilization of Normalized Coprime Factor Plant Descriptions with H_∞ Bounded Uncertainty," *IEEE Transactions on Automatic Control*, Vol. 34, No. 8, 1989, pp. 821–830.

[15]Hyde, R. A., and Glover, K., "The Application of Scheduled H_∞ Controllers to VSTOL Aircraft," *IEEE Transactions on Automatic Control*, Vol. 38, No. 7, 1993, pp. 1021–1039.

[16]Hyde, R. A., "H_∞ Aerospace Control Design—A VSTOL Flight Application," *Advances in Industrial Control Series*, Springer-Verlag, London, 1995.

[17]Walker, D. J., and Postlethwaite, I., " Advanced Helicopter Flight Control Using Two-Degree-of-Freedom H_∞ Optimization," *Journal of Guidance, Control, and Dynamics*, Vol. 19, No. 2, 1996, pp. 461–468.

[18]Walker, D. J., "Multivariable Control of the Longitudinal and Lateral Dynamics of a Fly-by-Wire Helicopter," *Control Engineering Practice,* Vol. 11, No. 7, 2003, pp. 781–795.

[19]Snell, S. A., Enns, D. F., and Garrard, W. L., "Nonlinear Inversion Flight Control for Supermaneuverable Aircraft," *Journal of Guidance, Control, and Dynamics*, Vol. 15, No. 4, 1992, pp. 976–984.

[20]"Application of Multivariable Control Theory to Aircraft Control Laws," Honeywell Technology Center and Lockheed Martin Skunk Works, WL-TR-96-3099, Wright–Patterson AFB, OH, May 1996.

[21]Menon, P. K., Iragavarapu, V. R., and Ohlmeyer, E. J., "Nonlinear Missile Autopilot Design Using Time-Scale Separation," Guidance, Navigation and Control Conf., AIAA Paper 97-3765, 1997.

[22]Korte, U., "Tasks and Needs of the Industrial Clearance Process," *Advanced Techniques for Clearance of Flight Control Laws*, edited by C. Fielding, A. Varga, S. Bennani, and M. Selier, Lecture Notes in Control and Information Sciences, No. 283, Springer-Verlag, Berlin, 2002, pp. 13–36.

[23]Packard, A., and Doyle, J., "The Complex Structured Singular Value," *Automatica*, Vol. 29, No. 1, 1993, pp. 71–109.

[24]Bates, D. G., Kureemun, R., and Mannchen, T., "Improved Clearance of a Flight Control Law Using μ-Analysis Techniques," *Journal of Guidance, Control, and Dynamics*, Vol. 26, No. 6, 2003, pp. 869–884.

[25]Horton, M. P., "Autopilots for Tactical Missles: An Overview," *Proceedings of the Institution of Mechanical Engineers, Part I, Journal of Systems and Control Engineering*, Vol. 209, No. 12, 1995, pp. 127–139.

[26]Vinnicombe, G., "Frequency Domain Uncertainty and the Graph Topology," *IEEE Transactions on Automatic Control,* Vol. 38, No. 9, 1993, pp. 1371–1383.

[27]Glover, K., Vinnicombe, G., and Papageorgiou, G., "Guaranteed Multi-Loop Stability Margins and the Gap Metric," *Proceedings of the IEEE 39th Conference on Decision and Control*, Vol. 4, IEEE Publications, Piscataway, NJ, 2000, pp. 4084–4085.

[28]Doyle, J., Glover, K., Khargonekar, P. P., and Francis, B. A., "State-Space Solution to Standard H-2 and H-Infinity Control Problems," *IEEE Transactions on Automatic Control*, Vol. 34, No. 8, 1989, pp. 831–847.

[29]Papageorgiou, G., and Hyde, R. A., "Analysing the Stability of NDI-Based Flight Controllers with LPV Methods," AIAA Guidance, Navigation and Control Conf., AIAA Paper 2001-4039, 2001.